Planetary and Space Science 58 (2010) 1945–1952

Contents lists available at ScienceDirect

Planetary and Space Science

journal homepage: www.elsevier.com/locate/pss

A new approach for estimating Titan's electron conductivity based on data from relaxation probe sensors on the Huygens experiment

Gregorio J. Molina-Cuberos [a,c,*], R. Godard [b], José J. López-Moreno [c], M. Hamelin [d], R. Grard [f], F. Simões [e,1], K. Schwingenschuh [g], V.J.G. Brown [c], P. Falkner [f], F. Ferri [h], I. Jernej [g], J.M. Jerónimo [c], R. Rodrigo [c], R. Trautner [f], M.J. Núñez [a], N. Ibrahim [i], C. Groth [i], M. Fulchignoni [j]

[a] Depto. Física, Facultad de Química, Campus Espinardo, Murcia, E30100, Spain
[b] Department of Mathematics and Computer Science, Royal Military College of Canada, Kingston (On.), Canada K7K 7B4
[c] Instituto de Astrofísica de Andalucía CSIC, P.O. Box 3004, 18080 Granada, Spain
[d] Université Versailles St Quentin CNRS/INSU LATMOS-IPSL, UPMC, 4, place Jusssieu, Paris, France
[e] LATMOS 4, Avenue de Neptune, 94107 Saint Maur, France
[f] RSSD, ESA-ESTEC, European Space Agency, Keplerlaan 1, 2200 AG Noordwijk, The Netherlands
[g] Space Research Institute, OEAW, Schmiedlstrasse 6, 8042 Graz, Austria
[h] CISAS, G. Colombo, Universitá di Padova, Via Venezia 15, 35131 Padova, Italy
[i] Institute for Aerospace Studies, University of Toronto, 4925 Dufferin Street, Toronto, Canada M3H 5T6
[j] LESIA, Observatoire de Paris, 5 Place Janssen, 92195 Meudon, France

ARTICLE INFO

Article history:
Received 19 May 2010
Received in revised form
13 September 2010
Accepted 14 September 2010
Available online 29 September 2010

Keywords:
Titan
Relaxation probe
Atmospheric electron conductivity
Space instrumentation

ABSTRACT

The Huygens Probe measured the electrical conductivity of Titan atmosphere from about 140 km down to the surface, employing relaxation and mutual impedance techniques. Previous analyses have shown some differences on the conductivity measurements obtained with two independent sensors—relaxation probe (RP) and mutual impedance probe (MIP). A 20-fold maximum discrepancy occurred around the conductivity peak at 60–70 km. To understand the nature of such discrepancy, we reassess the RP data by taking into account a geometrical factor related to the electrode finite size and the Debye length of the ionized medium. The present analysis implies replacing the standard Laplace field distribution by a more elaborated model considering the Poisson equation and the resistance between the RP electrodes and the medium. Although a complete understanding of the conductivity profile is still missing, this work brings RP and MIP data to a much better agreement. The conductivity maximum difference derived from the two sensors is now lower a factor of 2. This reassessment is also useful for future instruments and missions.

1. Introduction

The Huygens Atmospheric Structure Instrument (HASI), one of the six instruments on board Huygens, was designed to characterize the physical properties of the lower atmosphere and surface of Titan, the planet-size moon of Saturn (Fulchignoni et al., 2005). During the descent of the Huygens Probe, the Permittivity Wave and Altimetry (PWA) subsystem searched for the electrical conductivities due to positive ions and electrons, the complex permittivity of the environment, electric fields in the ELF and VLF ranges, lightning events, DC and quasi-static electric fields and acoustic signatures (Grard et al., 2006). PWA detected an ionized layer centered at an altitude around 63 km with two different instruments, the relaxation probe (RP) and mutual impedance probe (MIP) (Hamelin et al., 2007; López-Moreno et al., 2008). The MIP sensor also determined the relative permittivity and conductivity of Titan's surface material, whose preliminary lower estimates are 2 and $4\times10^{-10}\,\mathrm{S\,m^{-1}}$, respectively (Grard et al., 2006).

In preparation for the descent of Huygens on Titan, the HASI subsystems were previously tested in the Earth atmosphere during several balloon campaigns using Huygens Probe mock-ups (López-Moreno et al., 2002). Conductivity measurements made in the Earth stratosphere during balloon flights were compatible with results reported by other teams, thus validating RP-PWA correct functionality. However, comparisons among RP and MIP measurements were not possible due to the absence of electrons in the terrestrial atmosphere at balloon altitudes. The latter instrument is sensitive to electrons only.

On Earth, various techniques can be used to measure electron conductivity in the atmosphere, namely Gerdien condenser, mutual impedance, and relaxation (Hale, 1984; Croskey et al.,

* Corresponding author at: Depto. Física, Facultad de Química, Campus Espinardo, Murcia, E30100, Spain. Tel.: +34 868 887533; fax: +34 868 884148.
E-mail address: gregomc@um.es (G.J. Molina-Cuberos).
[1] Presently at NASA/GSFCC, Greenbelt, Maryland, USA.

0032-0633/$ - see front matter © 2010 Elsevier Ltd. All rights reserved.
doi:10.1016/j.pss.2010.09.014

1984, 2003). The relaxation technique, also known as transient method, allows development of simple, effective instrumentation. The experimental set-up consists of a simple electrode immersed in a medium that is artificially biased to a negative or positive potential with respect to a reference value. The classical theory assumes that (i) the potential distribution around the sensors obeys to Laplace equation ($\nabla^2 V = 0$), (ii) the ambient charges restore the initial equilibrium, and (iii) the electrode potential decays exponentially. However, Titan atmospheric conductivity measurements deduced from the RP sensor under these assumptions are significantly lower than those obtained by MIP. The classical theory of the relaxation method, which has been successfully applied in the Earth troposphere and stratosphere, cannot be applied to atmospheric environments where Debye length commensurate with probe dimensions. The effects resulting from the finite size of the electrodes, ambient DC electric field, and descent velocity through the atmosphere are not taken into account in the basic theory.

Cicerone and Bowhill (1969) were the first to emphasize the effect of the finite size of the electrode when radius is commensurate with the Debye length of charged particles. The Debye length, λ_D, is defined as $\lambda_D^2 = \varepsilon_0 K_B T/(N_e q_e^2)$, where ε_0 is the vacuum permittivity, K_B the Boltzmann constant, T the temperature, N_e the electron concentration, and q_e the electron charge. They examined theoretically the operation of a spherical electrostatic probe in a weakly ionized, collision-dominated gas and found an extreme sensitivity of the attracted current with respect to the Debye ratio, which is defined as $D_\lambda = a/\lambda_D$, where a is the electrode radius. The governing equations for the fluid model describing the collected current form a non-linear system comprising the continuity, flux, and Poisson equations for repelled and attracted species (Su and Lam, 1963). Numerical simulations are known to be extremely unstable because of the system of equations high sensitivity with respect to initial conditions and model parameterization. The work of Cicerone and Bowhill (1969) was followed by Chang and Kodera (1985) and Godard and Chang (1995), but their numerical results are too limited to be useful.

Huygens has provided evidence that the potential distribution around the electrodes follows Poisson rather than Laplace equation (López-Moreno et al., 2008). The probe was immersed in a collisional, weakly ionized medium, where the fraction of ionized molecules was always lower than 10^{-15}, with a subsonic turbulent velocity. Here we report a detailed analysis of electron conductivity derived from the RP measurements onboard Huygens and an associated numerical algorithm, which considers geometrical effects related to the finite size of the electrode and the Debye length of charged particles. RP sensors are widely utilized for terrestrial (Holzworth, 1981; Rosen et al., 1982; López-Moreno et al., 2001) and in planetary environments measurements (Hamelin et al., 2006; López-Moreno et al., 2008). Titan environment unique conditions allow us evaluating the RP sensors performance, relaxation theory validity, and RP and MIP comparative efficiency.

2. Electrical conductivity measurements techniques

The electrical conductivity sensors of the PWA subsystem were integrated in two deployable booms, and consisted of two disks (RP1, RP2) forming a double RP combined with four ring electrodes (RX1, TX1, RX2, TX2) composing the MIP quadrupole. Fig. 1 shows the arrangement of the electrodes in a deployed configuration with respect to the gondola and a close view of one boom holding the MIP and RP electrodes (Hamelin et al., 2007). The booms are made of glass fiber insulating material; RP1 and RP2 are mechanically similar. The connections run inside the

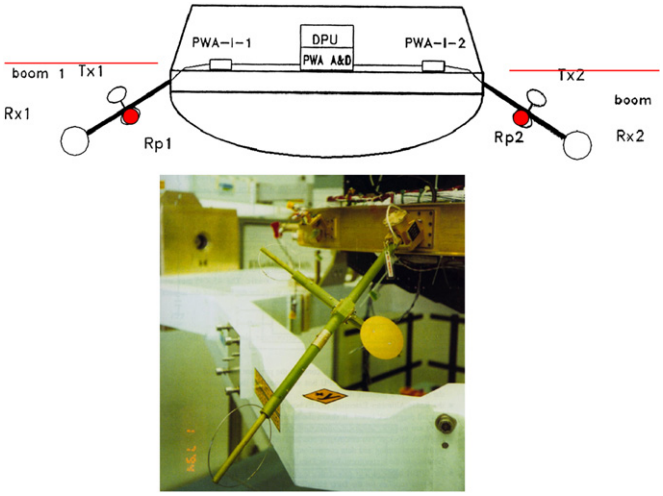

Fig. 1. The PWA electrode arrangement on Huygens. Top: sketch of the PWA sensors and electronics; the rings Tx1 and Tx2 are the transmitter electrodes; Rx1 and Rx2 are the receivers; the RP1 and RP2 disks are the RP electrodes. Bottom: close view of one boom with MIP and RP electrodes (Hamelin et al., 2007).

booms and comprise triaxial cables with the inner conductor connected to the electrode. The intermediate conductor is actively driven near the electrode potential and the outer connector is a grounded shield. Additional, detailed information about PWA architecture and boom configuration can be found elsewhere (Fulchignoni et al., 2002; Hamelin et al., 2007).

PWA was operating from an altitude of 141 km down to the surface, and during 32 min after landing. Part of the PWA data was lost due to the failure of one of the transmission channels between Huygens and the Cassini Orbiter (Lebreton et al., 2005). This data loss reduces MIP time resolution by a factor of 2. The RP1 data were lost and only the measurements performed with RP2, the electrode designed for large conductivities, are available.

2.1. The mutual impedance probe

The conductivity of a homogeneous and isotropic medium can be measured with an impedance probe. This instrument consists of four electrodes comprising one transmitting dipole (TX1–TX2) and one receiving dipole (RX1–RX2); the transmitting dipole is fed by an AC current generator. The ratio of the potential difference of the receiving electrodes to the injected current yields the resistance of the medium, provided its homogeneity is perturbed neither by the injected current nor by the dipole itself. This situation is generally never encountered in electrolytes and plasma because charged sheaths form around the electrodes. Therefore, complementary studies were necessary to improve the Titan MIP data. Additional laboratory tests were performed to validate or improve the calibration results. Temperature effects were included and numerical models of the MIP sensors and electric circuitry have been developed to take into account the proximity of the Huygens Probe body. The effect of the vertical motion of the vessel in the ionized atmosphere is estimated in both analytical and numerical ways (Hamelin et al., 2007).

The electron concentration is derived from combining the conductivity measured by PWA with the neutrals density and temperature (Fulchignoni et al., 2005). These quantities are linked to the electron conductivity σ_e as follows (Banks and Kockarts, 1973):

$$\sigma_e = N_e \frac{q_e^2}{2.33 \times 10^{-17} N_n T m_e}, \quad (1)$$

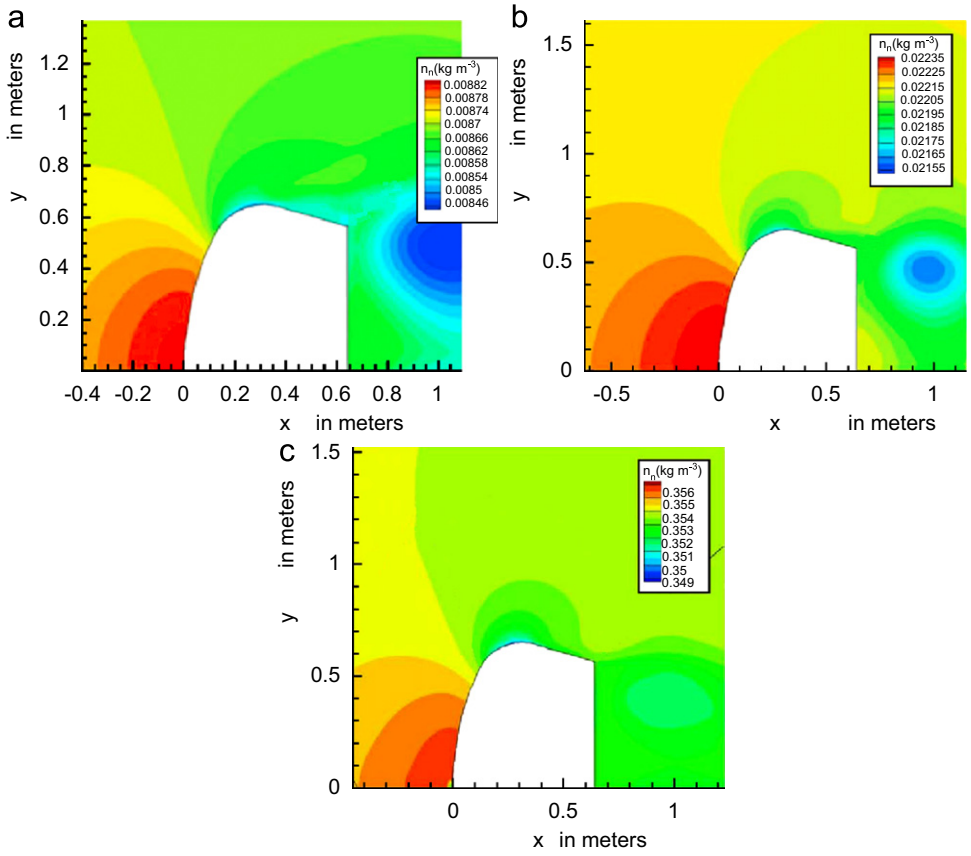

Fig. 2. Neutral density n_n (in kg m^{-3}) for the Huygens Probe in a turbulent flow at the altitudes of 130, 100 and 50 km. The flow velocity is parallel to the X axis, and dimensions of the Huygens Probe are in meters.

where m_e is the electron mass and N_n the neutrals number density. We have verified numerically, by running a turbulence model, that the neutrals number density, at the position of the MIP or the RP devices, is not affected by the shadowing effect of the vessel (Ibrahim, 2009). For example, Fig. 2 shows contour maps of the neutrals density n_n at three different altitudes: 130, 100, and 50 km. There is almost no difference between the upstream and the downstream regions of the vessel. Therefore, we have great confidence in MIP electron concentration estimates.

In the first part of the descent, above 110 km before the main parachute releasing, the MIP data are found inconsistent with a nominal response (Hamelin et al., 2007) and the passive ELF measurements are nearly similar to the noise level observed during the cruise phase (Simões et al., 2007). A probable explanation is that one or, less likely, both booms were not fully deployed during the mentioned period. Therefore, MIP data above 100 km were not analyzed. Table 1 shows the altitude profile of electron conductivity and derived electron concentration, and Debye ratio obtained by MIP, where the altitude is reported by Kazeminejad et al. (2007). The Debye ratio allows for a comparison between the electrode radius and the effective shielding length of a charged particle.

Table 1
Electron conductivity and electron concentration from MIP (Hamelin et al., 2007), and associated Debye ratio, D_λ.

Altitude (km)	σ_e (nS m^{-1})	N_e (cm^{-3})	D_λ
100	0.160	10.7	0.14
88.5	0.136	12.8	0.16
78.9	0.056	12.4	0.16
78.7	0.251	31.2	0.26
70.9	1.81	283	0.84
70.8	2.14	335	0.92
62.9	3.00	647	1.44
62.8	3.04	659	1.45
60.3	2.48	625	1.50
60.2	2.44	616	1.49
56.0	1.16	378	1.16
55.9	1.23	399	1.19
52.2	0.561	227	0.90
52.2	0.517	210	0.87
48.9	0.293	145	0.72
48.9	0.340	168	0.78
45.0	0.200	125	0.67
42.3	0.284	208	0.86
42.3	0.181	133	0.07

2.2. Relaxation probe—the Laplace approximation

The experimental set-up of the relaxation probe consists of an electrode exposed to the ionized medium that is biased at a negative or positive potential with respect to a reference level, the Huygens Probe structure. The electrode, a circular disk of radius $a=3.5$ cm, is mounted on a boom at a distance of 15 cm from the gondola. The sensor subsequently returns to its initial equilibrium potential by collecting positive or negative ambient charges. The sequence of measurements consists of four relaxation cycles of 56 s, where the source potential is successively set to +5, 0, −5, and 0 V. When the electrode is biased with respect to the reference potential, it collects a current produced by the attracted species. For atmospheric experiments, this current is produced by several terms: diffusion, convection, external electric field, and electrode potential gradient.

The diffusion term is related to number density gradients close to the surface of the electrode in the undisturbed medium. It is driven by the thermal velocity of electrons, which is $\approx 50\,\mathrm{km\,s^{-1}}$. The convection term is related to the descent velocity of the system, of the order of a few $10\,\mathrm{m\,s^{-1}}$. The electrode gradient term, about $\approx 200\,\mathrm{V\,m^{-1}}$ close to the electrode when charged at 5 V, produces an electron drift velocity much greater than a few $\mathrm{km\,s^{-1}}$. As a result, convection can be neglected and the probe remains stationary with respect to the electronic fluid. The natural electric field also induces a small current. Grard et al. (2006) estimated an upper limit for the upward electric field $E_z \approx 1\,\mathrm{V\,m^{-1}}$, which is negligible compared to the electrode gradient term. Additionally, when the electrode is positively biased, all photo-electrons are returning back to the surface, and they should not contribute to the current. The electrode potential gradient is indeed the dominant term.

Assuming that the electrode is biased to a potential V, the current is directly proportional to the electric potential gradient around the electrode. Then, for a conducting electrode, the medium is collisional, very weakly ionized, and the potential around the electrode can be described by the Laplace equation

$$\nabla^2 V = 0, \tag{2}$$

and the boundary conditions are

$$V(r=a,t) = V_a(t) \tag{3}$$

$$V(r\to\infty,t) = 0, \tag{4}$$

where $V_a(t)$ is the electrode potential. Here, for the sake of simplicity and historical reasons, we assume that the electrode possesses spherical symmetry. If the electrode is a disk, such as on Huygens, we can apply a conformal map to switch from one geometry to the other. A conformal map is used to transform spherical into cylindrical geometries via the correction factor K, which is 1 for a sphere and $2/\pi$ for a disk. Therefore, we shall consider a spherical geometry, which corresponds to a one-dimensional solution, rather than a disk geometry, a more complex two-dimensional numerical problem.

For a spherical electrode embedded in an homogeneous medium, the concentration of attracted particles $N_e(r=a,t)$ is always equal to the undisturbed charge concentration $N_e(r\to\infty,t) = N_{e,\infty}$. In this case, the inward current I_a is given by (Mozer and Serlin, 1969; Kellog and Weed, 1969; Godard, 2007)

$$I_a(t) = 4\pi K a^2 \sigma_a \left\| -\frac{dV(r,t)}{dr} \right\|_{r=a}, \quad V(r,t) = V_a(t)\frac{a}{r} \tag{5}$$

$$I_a(t) = 4\pi K a \sigma_a V_a(t) = \frac{V_a(t)}{R_a}, \tag{6}$$

where σ_a is the electric conductivity for attracted species, $\|-dV/dr\|_{r=a}$ the electric field strength on the electrode surface, r the radial distance, and R_a the effective resistance of the electrode in the ionized medium.

On the other hand, the RP theory is also directly linked to the theory of electrostatic probes in a slightly ionized, collision-dominated gas where an electrode or any object acts as a particle sink with $N_e(r=a,t) = 0$ at the electrode surface (Cicerone and Bowhill, 1969; Swift and Schwar, 1969; Godard, 2007). In particular, Swift and Schwar (1969, pp. 177–181) commented in detail the derivation of the boundary condition $N_e(r=a,t)=0$ and the influence of the mean free path. It is clear that exact boundary conditions in any model involving differential equations are directly linked to the well-posedness of the problem. If the RP potential is zero, the only electron or ion density perturbations in the electrode vicinity would be due to diffusion, convection, and to the geometry of the electrode itself. In the case of Huygens, we verified that convection dominates. Therefore, results for the neutral flow could reasonably be extended to electrons or ions (Ibrahim, 2009). This means the electron density would be uniform around the vessel, provided that it was at zero potential; we can then assume $N_e(a_V,t) = N_e(r\to\infty,t)$, where a_v would be the equivalent vessel radius. Since the RP disk is small and roughly oriented in the direction of the flow, the diffusion and convection currents are similar when a zero electrode potential applies. We have verified that for a Laplace model, because of its linearity, the collection of current, and consequently the RP potential decay, is independent of the electron concentration boundary condition at the electrode surface. In fact, if we choose $N_e(r=a,t) = \alpha N_e(r\to\infty,t)$, where α is in the range $0 \le \alpha \le 1$, almost identical results are obtained. Because this work is focusing on the data processing rather than in new developments of mathematical models for RP, we shall omit a lengthy demonstration of the above result. However, this important result is not true for a Poisson field, which corresponds to a non-linear model (Godard et al., 2010).

Let us now consider the signal from the RP sensor. For a Laplace potential, the Debye ratio is equal to zero, and the free space capacitance around the electrode is constant. For a disk or a sphere simplified model, we find

$$\frac{\sigma_a}{\varepsilon_0} = \frac{1}{R_a C_a}, \tag{7}$$

where C_a is the electrode capacitance.

If the reference potential is stable, the potential difference between the RP electrode and the Huygens vessel follows the exponential law

$$V_a(t) = (V_0 - \Delta V_f)e^{-t/\tau} + \Delta V_f, \tag{8}$$

where V_0 and ΔV_f are the initial and floating potentials, respectively. The slope of the potential decay, or time constant τ, is related to the resistance and capacitance of the electrode in the plasma by $\tau = R_a C_a$ and provides the polar components of the electrical conductivity

$$\sigma_a = \frac{\varepsilon_0}{\tau}. \tag{9}$$

In order to reduce the speed of decay of the electrode potential for a given conductivity, thus extending the range of measurements towards larger conductivities, a discrete capacitor $C_* = 352.5$ pF was connected in parallel with the RP2 sensor. Under these conditions, the global capacitance is replaced by $C_* + C_a$, and the time constant becomes

$$\tau = R_a(C_* + C_a) = \frac{C_* + C_a}{C_a}\frac{\varepsilon_0}{\sigma_a}. \tag{10}$$

At this stage, and we would like to emphasize it again, this classical model of RP gives, in some cases, a 20-fold discrepancy with respect to MIP results.

2.3. Relaxation probe—the Poisson approximation

If the size of the electrode is comparable to the Debye length, the resistance and the capacitance of the system RP-medium are modified and they are functions of the applied potential. In order to consider a reasonable computational approach, let us consider a quasi-static approximation for a slowly time varying problem. Assuming an instant stationary solution, it is easier to compute the electrode current for a given potential. Therefore, we can build a set of I–V characteristic functions and compute the resistance vs. potential or time. By interpolation, it is possible building a continuous set of resistances and capacitances for various Debye ratios. Now we replace (2) by Poisson equation

$$\nabla^2 V = -\frac{q_e}{\varepsilon_0}(N_+ - N_-), \tag{11}$$

where N_+ and N_- are the concentration of positive and negative charges (mainly electrons in the case of Huygens), respectively. To solve Eq. (11) it is necessary to compute, simultaneously, the basic fluid equations

$$\mathbf{\Gamma}_\pm = -\mathcal{D}_\pm \nabla N_\pm \mp \mu_\pm N_\pm \nabla V,$$

$$\nabla \cdot \mathbf{\Gamma}_\pm = 0, \tag{12}$$

where $\mu_\pm$ and $\mathcal{D}_\pm$ are the mobility and diffusion coefficients, respectively, and $\mathbf{\Gamma}$ is the particle flux number density. The flux equations are linked to the boundary conditions

$$N_\pm(r=a) = 0$$

$$\lim_{r\to\infty} N_\pm(r) = N_\infty. \tag{13}$$

For the sake of simplicity, and to keep the same notation used by Cicerone and Bowhill, we consider $N_- = N_e$. The classical boundary conditions at the electrode surface are known from collisional electrostatic probe theory. We refer to Swift and Schwar (1969) for a derivation as a function of pressure. A review of the theories governing the collection of charges by biased probes and the numerical solution for several values of the relevant parameters can be found in Cicerone and Bowhill (1969). They suggested power-law fits for the I–V characteristics. Results are presented as a function of dimensionless potential φ, defined as the ratio of the electric potential energy with respect to the thermal energy $\varphi = V_0 q_e/(K_B T)$, for a Debye ratio in the range $0.1 < D_\lambda < 1$. For the Huygens conditions, it is necessary to interpolate and extrapolate the results. Fig. 3 shows the dimensionless current as a function of the Debye ratio for $\varphi = 500$. We observe that the values follow a linear correlation in a double logarithm scale. From physical considerations and perturbation theory, the derivative of the current with respect to D_λ and at D_λ must be zero, and a linear relation is not valid. For low D_λ, in the range $0 < D_\lambda < 0.1$, we have obtained the dimensionless inward electron current considering Hermite interpolation. Fig. 4 shows the normalized dimensionless inward current with respect to the diffusion value $4\pi a N_e q_e \mathcal{D}_e = 4\pi\sigma_e K_B T/q_e$ as a function of $|\varphi|$ for various Debye ratios. The diffusion value corresponds to the case where the electrode potential is zero, and the diffusion current is only due to electron concentration gradients. Here we assume that the Einstein relation for diffusion, $\mathcal{D}_e = \mu_e K_B T/q_e$, is valid, and the data from Hasted (1964) suggest that it should be aborderline case; μ_e is the electron mobility. We observe the classical decrease of the inward current density as the Debye ratio increases and a slow variation

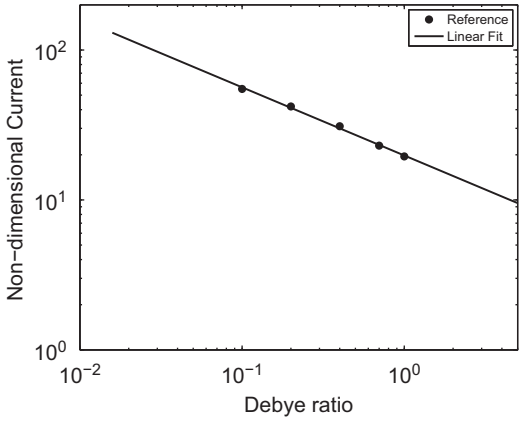

Fig. 3. Dimensionless current as a function of the Debye ratio for $\varphi = 500$ as reported by Cicerone and Bowhill (1969) and double logarithm fit.

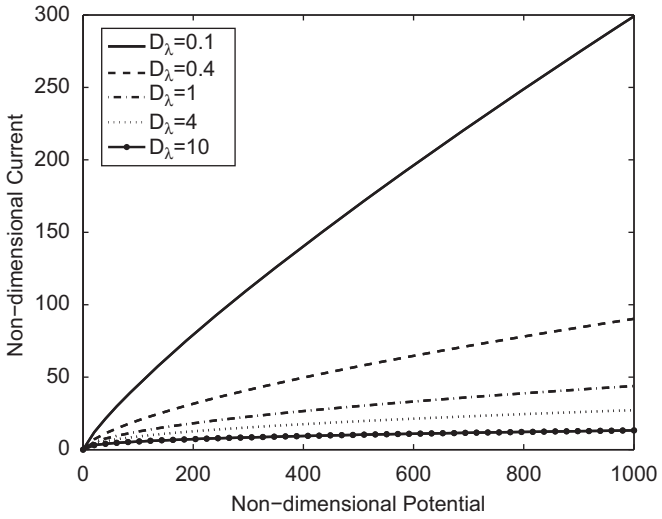

Fig. 4. Interpolated/Extrapolated values of the dimensionless inward current density from power-law formulas vs. dimensionless spherical electrode potential, for various Debye ratios. The inward current is normalized with respect to the diffusion current $4\pi a N_e q_e \mathcal{D}_e$.

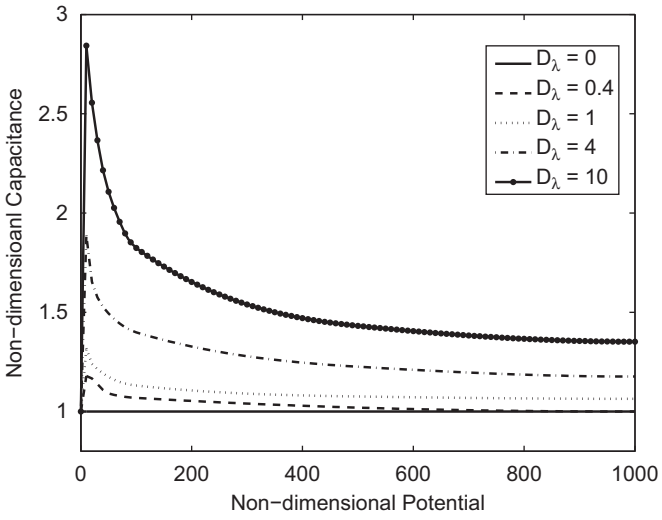

Fig. 5. Dimensionless spherical electrode capacitances vs. dimensionless potentials, φ, for various Debye ratios. Capacitances are normalized with respect to their values in vacuum.

of the current for large values of D_λ. The current seems to saturate for $D_\lambda > 4$. For a more accurate RP data processing, it is necessary to take into account the fact that the resistance and capacitance of the electrode are functions of the electrode potential and Debye ratio.

Because of the supplementary capacitance C_*, which is much higher than the electrode capacitance, the data processing for Huygens RP sensors does not require the computation of the electrode capacitance in the ionized medium. Even if the calculation of C_a is unnecessary, we have obtained a first order computation of the capacitance of the electrode-plasma system (see Godard, 2007 for details). Fig. 5 shows the dimensionless spherical electrode capacitances with respect to values in vacuum, for various values of the Debye ratio. We observe a slow decay of capacitances for large potentials. In the limit of a zero Debye length, and for large attracting potentials, the capacitance approaches the solution in vacuum.

Considering Figs. 4 and 5, it is possible to simulate a relaxation signal with different input parameters, namely descent velocity, negative ion conductivity, or the reference potential.

The theoretical potential signal V_{th} between the RP electrode and the medium satisfies the following equation

$$I=\frac{dQ}{dt}=\frac{d}{dt}(CV_{th})=-\frac{V_{th}}{R} \tag{14}$$

where I is the collected current and Q is the charge of the electrode; the RP signal is then written

$$\frac{dV_{th}}{dt}=-\frac{V_{th}}{RC}-\frac{V_{th}}{C}\frac{dC}{dV_{th}}\frac{dV_{th}}{dt}\Rightarrow$$

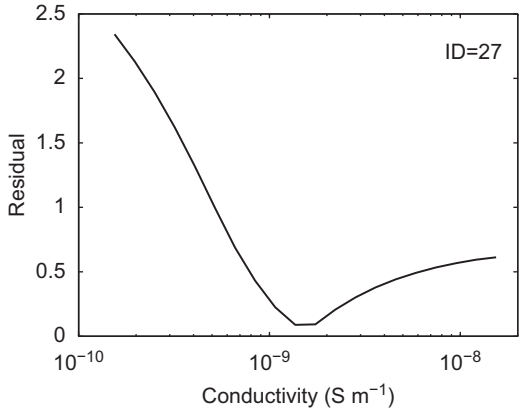

Fig. 6. The total residual of the minimization process as a function of electron conductivity. This example is calculated for the maximum conductivity, at 63.3 km.

$$\frac{dV_{th}}{dt}=-\frac{V_{th}}{RC\left(1+\frac{V_{th}}{C}\frac{dC}{dV_{th}}\right)}, \tag{15}$$

with the initial condition $V_{th}\,(t=0)=5$ V. Eqs. (10–15) constitute the mathematical model for the equivalent R–C network for the RP sensor.

Note that Eq. (15) is a stiff differential equation, which is solved through an implicit Eulerian backward scheme. In the Huygens experiment, as mentioned previously, a dominant shunt capacitance C_* is connected in parallel with the RP2 sensor; consequently, the finite difference signal is

$$V_{th}(j)=\frac{V_{th}(j-1)}{1+\frac{h}{C_*R(j-1)}}, \tag{16}$$

where j is the iteration index and h the time step.

First, the signal is simulated numerically with a guessed electron concentration. Then, results from Fig. 4 are input parameters for the calculation of the resistance. These outputs are then used to solve Eq. (16). Finally, the electric conductivity is adjusted by calculating the minimum of the residual function, $\mathcal{R}$, defined as the sum of the least absolute deviations according to

$$\min(\mathcal{R}(\sigma_e))=\frac{1}{n}\sum_{i=1}^{n}|V_{th}(t_i,\sigma_e,D_\lambda)-V_{meas}(t_i)|, \tag{17}$$

where n is the number of observations and $V_{meas}(t_i)$ the experimental data. The inferred conductivity is then found by residual minimization. We find Eq. (17) an appropriate method because it reduces the weight of large residuals. Fig. 6 shows an example of the residual $\mathcal{R}$ as a function of the electron conductivity obtained at an altitude of $\approx$63 km. This minimization function is unimodal, and forms a cusp near the global

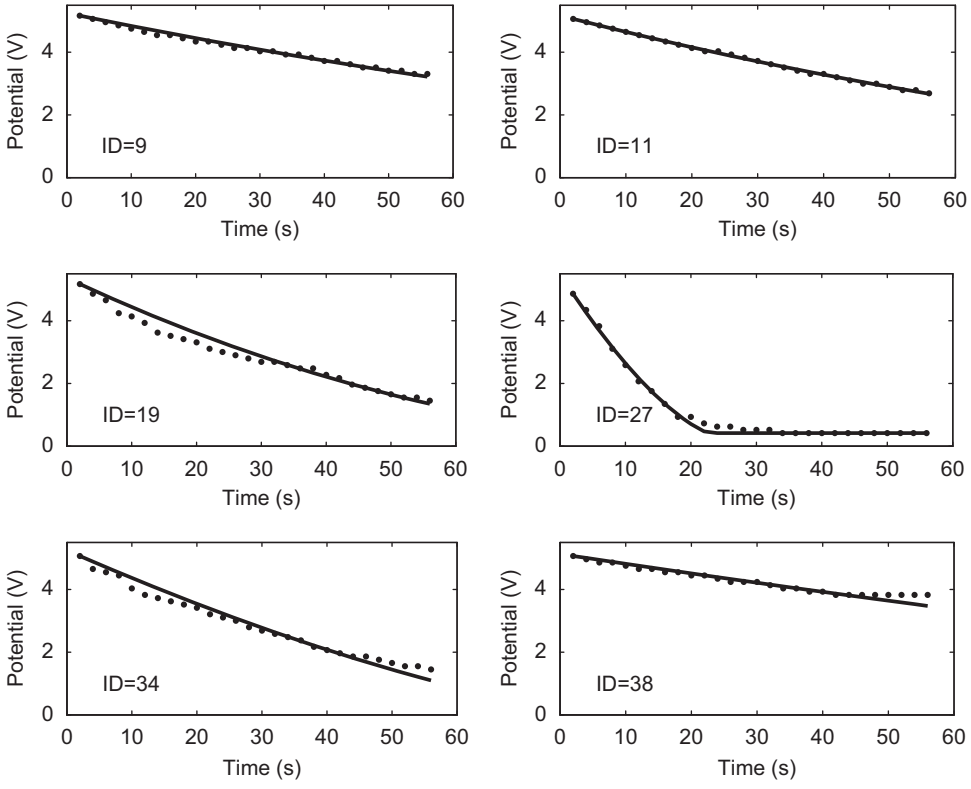

Fig. 7. Typical relaxations for the electrode biased at $V_0=5$ V. The fitting line is obtained by solving Poisson equation, where ID is the packet number. Altitude and other parameters are shown in Table 2.

minimum. We have performed a straightforward one variable half interval search.

3. Results and discussion

Fig. 7 shows six relaxation cycles obtained when electrons are attracted, $V_0 = 5$ V; the fitting lines are computed by solving Poisson equation. We observe very good fits between experimental and simulated data. Table 2 shows the altitude and electron conductivity for each relaxation cycle of Fig. 7. The electron conductivity obtained by MIP is also shown for comparison (Hamelin et al., 2007). The conductivity derived from RP, including our minimization technique for a Poisson field, agrees reasonably well with the measurements provided by MIP. We have also observed that the electron conductivity obtained by means of minimization algorithm, Eq. (17), is very sensitive to the collected electron current. At this stage, we do not know if the difference originates from MIP or RP analysis. We do not question the scientific validity of Cicerone and Bowhill work, because their results coincide with those obtained by other algorithms. However, it is possible that our interpolation/extrapolation scheme introduces additional errors, especially at small Debye ratios. For the sake of comparison, the conductivity obtained by assuming a Laplace field at the peak is about 20 times lower than that provided by the MIP sensor.

Table 3 shows the electron concentration, electron conductivity, and Debye ratio for all the relaxation cycles. Note that the ambient electron concentration is not necessarily accurate close to the electrode, and we may have a more complex relationship at the vicinity of the electrode with possible shadowing effects from the gondola, especially if the boom was not completely deployed above 110 km as proposed by Hamelin et al. (2007). We observe very small Debye ratios at high altitudes, from 134 km down to 70 km; below these altitudes, the Debye ratio is larger. We found similar patterns from MIP results. From the electron concentration profiles shown in Fig. 8, we find that MIP and RP measurements follow a similar pattern.

Table 2
Electron conductivity calculated with Laplace and Poisson approximations for the packet numbers ID=7, 11, 19, 27, 34, and 38. The electron conductivity obtained by MIP is also shown for comparison (Hamelin et al., 2007).

ID	Altitude (km)	RP: Laplace	RP: Poisson	MIP	
		σe[a]	σe[a]	σ_e[a]	D_λ
7	123	0.010	0.034	–	–
11	114	0.015	0.051	–	–
19	84	0.031	0.26	(0.14–0.25)[b]	0.16–0.26
27	63	0.133	2.06	3.0	1.4
34	52	0.053	0.49	0.54	0.9
38	48	0.031	0.14	0.32	0.7

[a] Units are in nS m^{-1}.
[b] Conductivity values at 88.5 and 78.7 km, respectively. A very low value (0.056 nS m^{-1}) is also measured at 78.9 km.

Table 3
Conductivity, electron number density and Debye ratio from the relaxation probe sensor assuming a Poisson field for the potential.

Altitude (km)	σ_e (nS m^{-1})	N_e (cm^{-3})	D_λ
135	0.033	0.82	0.04
123	0.034	0.99	0.04
114	0.051	2.0	0.06
084	0.26	28	0.24
73	0.53	87	0.45
71	1.8	290	0.83
63.3	2.1	48	1.2
57.9	1.0	33	1.07
57.3	0.63	21	0.86
52.2	0.49	22	0.89
47.7	0.14	80	0.54
43.8	0.021	16	0.24

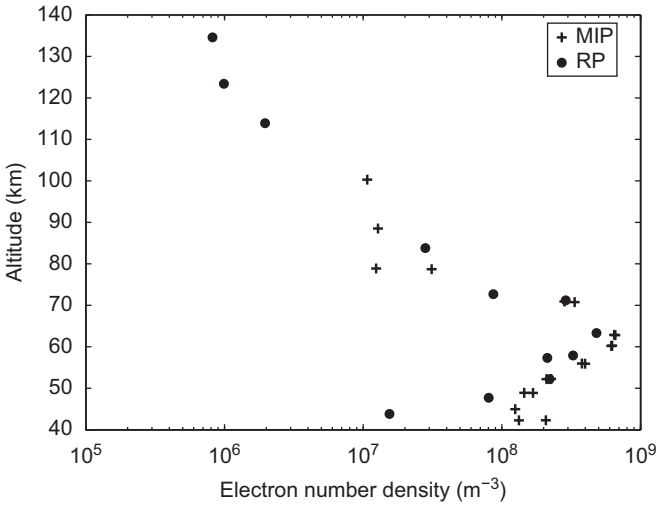

Fig. 8. Electron number density obtained by MIP and RP.

4. Conclusions

Because two independent techniques are used to investigate the atmospheric conductivity during the descent of the Huygens Probe on Titan, comparison between RP and MIP measurements is possible. The measurements obtained by the RP sensor on Huygens indicate a geometrical effect related to the ratio of the size of the electrode to the Debye length of charged particles. Using a similar approach to that of Cicerone and Bowhill and a conformal mapping of a sphere into a disk, we are able to reduce the difference between MIP and RP results from a factor of 20 to roughly a factor of 2. To understand whether a better agreement between RP and MIP measurements is possible, it is our intention to keep refining the conductivity retrieval method with a more elaborated numerical simulation that also includes shadowing effects between the gondola and the RP sensor.

Acknowledgments

The authors would like to acknowledge the invaluable discussions and suggestions made by C. Béghin of the LPCE-CNRS and J.J. Berthelier of the CETP-IPSL. This work was supported by contracts ESP2003-00357, ESP2006-02934, AYA2009-08190 (Ministerio de Ciencia y Tecnología, Spain) and 11844/PI/09 (Fundación Séneca, Región de Murcia, II PCTRM 2007–2010 framework). The authors thank all the national and international institutions that made the success of this experiment possible and especially International Space Science Institute for hosting their working-team meetings.

References

Banks, P., Kockarts, G., 1973. Aeronomy. Academic Press, New York.
Chang, J.-S., Kodera, K., 1985. Theory of electric conductivity measurements by an electrostatic probe in an atmospheric low-density continuum ionized gas. J. Geophys. Res. D 90, 5897–5900.

Cicerone, R.J., Bowhill, S.A., 1969. Theory of ion collection by a stationary electrostatic probe. Radio Sci. 4, 561–571.
Croskey, C.L., et al., 1984. Electrical structure of PMSE and NLC regions during the DROPPS program. Geophys. Res. Lett. 28 (8), 1427–1430.
Croskey, C.L., Mitchell, J.D., Friedrich, M., Investigation of atmospheric neutral constituents by photoionization techniques. In: ESA-SP 530, 2003, pp. 395–400.
Fulchignoni, M., et al., 2002. The characterisation of Titan's atmospheric physical properties by the Huygens Atmospheric Structure Instrument (HASI). Space Sci. Rev. 104, 395–431.
Fulchignoni, M., et al., 2005. In situ measurements of the physical characteristics of Titan's environment. Nature 438, 785–791.
Godard, R., 2007. Sheath and potential profiles around RP sensors and the gondola in the Huygens experiment. In: Dravid, V. (Ed.), Proceedings of the COMSOL conference, Burlington, USA, pp. 225–232.
Godard, R., Chang, J.K.K., 1995. Validity of the theories for the measurement of electric fields and conductivity in the stratosphere. Tokyo Denki Univ. J. 43, 7–21.
Godard, R., De Boer, J., Ibrahim, N., Molina-Cuberos, G., 2010. Electrostatic fluid structure interaction (EFSI) on the Huygens experiment. In: COMSOL Conference Proceedings, Boston.
Grard, R., et al., 2006. Electric properties and related physical characteristics of the atmosphere and surface of Titan. Planet. Space Sci. 54, 1124–1136.
Hale, L.C., 1984. Middle atmosphere electrical structure, dynamics and coupling. Adv. Space Res. 4 (4), 175–186.
Hamelin, M., et al., 2006. ARES: an atmospheric electricity instrument proposed for EXOMARS. Results of balloon tests in the terrestrial atmosphere. In: European Planetary Science Congress, p. 528.
Hamelin, M., et al., 2007. Electron conductivity and density profiles derived from the mutual impedance probe measurements performed during the descent of Huygens through the atmosphere of Titan. Planet. Space Sci. 55, 1964–1977.
Hasted, J., 1964. Physics of Atomic Collisions. Butterworths, London.
Holzworth, R.H., 1981. High latitude stratospheric electrical measurements in fair and foul weather under various solar conditions. J. Atmos. Terr. Phys. 43, 1115–1125.
Ibrahim, N., 2009. CDF Analysis of Huygens probe In Titan's Atmosphere. University of Toronto, Institute for Aerospace Studies, Toronto, Unpublished Thesis.
Kazeminejad, B., Atkinson, D.H., Pérez-Ayúcar, M., Lebreton, J.-P., Sollazzo, C., 2007. Huygens' entry and descent through Titan's atmosphere. Methodology and results of the trajectory reconstruction. Planet. Space Sci. 55, 1845–1876.
Kellog, P.J., Weed, W.M., 1969. Balloon Measurements of the Ionospheric Electric Fields. Planetary Electrodynamics, vol. 2. Gordon and Breach Science Publishers.
Lebreton, J.-P., et al., 2005. An overview of the descent and landing of the Huygens probe on Titan. Nature 438 (7069), 758–764.
López-Moreno, J.J., Molina-Cuberos, G.J., Rodrigo, R., Hamelin, M., Schwingenschuh, K., 2001. Polar ionic conductivity profile in fair weather conditions. Terrestrial test of the Huygens/Hasi-PWA instrument aboard the Comas Sola balloon. J. Atmos. Sol.-Terr. Phys. 63, 1959–1966.
López-Moreno, J.J., et al., 2002. The Comas sola mission to test the HUYGENS/HASI instrument on board a stratospheric balloon. Adv. Space Res. 30, 1359–1364.
López-Moreno, J.J., et al., 2008. Structure of Titan's low altitude ionized layer from the relaxation probe onboard HUYGENS. Geophys. Res. Lett. 35, L22104.
Mozer, F.S., Serlin, R., 1969. Magnetospheric electric field measurements with balloons. J. Geophys. Res. 74, 4739–4754.
Rosen, J.M., et al., 1982. Results of an international workshop on atmospheric electrical measurements. J. Geophys. Res. 87, 1219–1224.
Simões, F., et al., 2007. A new numerical model for the simulation of ELF wave propagation and the computation of eigenmodes in the atmosphere of Titan: did Huygens observe any Schumann resonance? Planet. Space Sci. 55 1978–1989.
Su, C.H., Lam, S.H., 1963. Continuum theory of spherical electrostatic probes. Phys. Fluids 6, 1479–1491.
Swift, J.D., Schwar, M.J.R., 1969. Electric Probes for Plasma Diagnostics. London Iliffe Books, London.